LABORATORY REPORT 4
Imaging Obscured Star Clusters in the Infrared

Kirsten Howley [1]
Group 2
November 13, 2001

1. BACKGROUND & MOTIVATION

The ability to determine the secrets of our neighbors in the Milky Way Galaxy is an exploration into how much information we can gather from tiny photons received from these distant objects. It is surprising, and amazing, how much information we can indeed obtain from these little packets sent to us.

One significant source of information is stellar clusters. Stellar clusters are created during the gravitational collapse of molecular clouds. Population I clusters, known as open clusters, tend to be small and young, in comparison to the older globular clusters which formed when the Galaxy was young. Clusters offer a good test to the theories of the time scale of stellar evolution. Since the most massive stars ascend the main sequence first, and have the shortest lifetimes, determining the types of stars populating a cluster can can also reveal the age of the cluster.

The gas and dust that forms these stellar clusters is scattered throughout our galaxy. These grains absorb more efficiently in the bluer wavelengths. For this reason, it is more efficient to study stellar evolution in the infrared, where less of the photons are absorbed during their journey to our telescope. Stars viewed through these dust grains appear to be more red (thus the term reddening). The reddening in the stars is caused by the higher absorption of higher energy photons.

2. EQUIPMENT & METHOD

The Leuschner 30-inch telescope, which operates on celestial coordinates was used to obtain infrared images. Taking images from the Leuschner telescope and infrared camera involved a remote login to the system 128.32.197. Once in the system, the dome needed to be opened and positioned to look out the slit, a filter need to be selected (the K filter, H filter, J filter, and aluminum plug were used for this lab), the flip mirror had to be opened, and the telescope had to be focused and pointed at the desired location. Since the Leuschner telescope operates on celestial coordinates, one needed to verify that the desired object was presently within viewing range (above the horizon) before imaging an object. Images were taken with selected exposure times using the *qimage* command. Files were exported from the remote system into the local system using *sftp*. Detailed log sheets were kept for images collected from the telescope, and can be accessed at enielsen/lab04/logsheets/.

[1] E-mail: kirsten@ugastro.berkeley.edu

3. DATA COLLECTION & ANALYSIS

Our group chose to observe the galactic star forming region NGC 1333 located at a distance of 320 parsecs, with celestial coordinates of 03:29:02.00 RA and +31:20:54.0 DEC. The cluster was observed at J, H and K wavelengths, or 1.25 μm, 1.65 μm, and 2.20 μm, respectively. First, 27 images of the cluster were taken in a rastered pattern, offset by .01 degrees (approximately 27 pixels) for each subsequent image. 27 Images of standard stars were also taken in a rastered pattern; GSPC P247-U, HD 18881, SAO 038218, and SAO 056596 0, 1 & 2 were the chosen standard stars. A control field was also selected to represent an average portion of the sky to compare to the cluster. The coordinates of our control field were 03:53:45 RA and +37:14:10 DEC. Again, 27 rastered images of our control field were taken.

After data was collected, images were dark subtracted, flat fielded, sky subtracted and assembled into a mosaic at each wavelength. The mosaics were created by first shifting the rastered images of our cluster, using the same star in each of the frames as a reference point, and combining them into a super array where the selected star from each 256 x 256 image was shifted to reside at the same point in the super array. Then, since some of the pixels in the detector were either cold, warm or hot pixels, and thus registered unreliable information, a bad pixel mask was created. Pixels that alway registered high counts (hot pixels) were defined as pixels which recorded counts greater than three standard deviations from the median of a median dark image (created from 25 dark images). Pixels that always registered low counts (cold pixels) were defined as pixels which recorded counts less than three standard deviations from the median of our flatfield images. The locations of these pixels were noted, and were assigned a zero value in a 256 x 256 array, where all other pixels were valued at 1. The bad pixel mask was shifted in exactly the same pattern as each of the cluster images, so that we ended up with 27 separate bad pixel mask images. In each image, both the bad pixels and the pixels surrounding the area representing pixels exposed to the detector were given a value of zero. Each of these bad pixels masks were multiplied by their corresponding (shifted) cluster image to get rid of the bad pixels. The bad pixel masks were then added together to created a mosaic which represented the total exposure time for each pixel. Zero values were assigned a large negative value, so when dividing you would get a very small number close to zero. Using these values as a weighted mean, the final mosaic was constructed:

$$x_w = \frac{\sum_{i=0}^{N} w_i x_i}{\sum_{i=0}^{N} w_i}$$

where x_w corresponds to our final mosaic image, w_i corresponds to each individual (shifted) bad pixel mask, and x_i represents each individual (shifted) cluster image.[2]

The advantage of assembling dithered images into a mosaic is that it effectively increases exposure time, which allows us to view dimmer stars, increases the signal to noise ratio, and increases the amount of sky viewed. This was especially effective in viewing dim stars in the K-band, where our detector saturates quickly. Our final super array image was 360 x 375 pixels, or

[2]Taylor, John R.

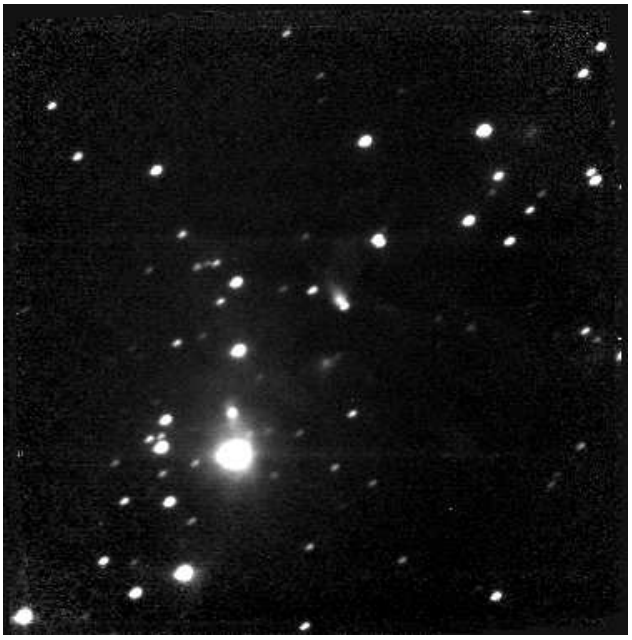

Fig. 1.— NGC 1333 combined infrared mosaic in J, H, & K.

8.1 x 8.4 arcseconds. Figure 1 depicts our added mosaics in J, H and K bands.[3]

Photometry was performed on the mosaic. An circular aperture with a four pixel radius was used to convolve the mosaic. The signal was extracted with the circular tophat, and an adjacent moat collected and subtracted the neighboring sky signal. The aperture used is displayed in Figure 2. Convolving the image involved placing our aperture over each pixel in the mosaic, integrating over the aperture, and placing that value in the center pixel. This essential converted our Gaussian distribution into a Dirac Delta Spike, or a response into a stimulus. Our response, $\phi(x, y)$, which are the spread out photons received from our star is given by:

$$\phi(x,y) = \frac{1}{2\pi\sigma_x\sigma y} e^{-\frac{1}{2}[(\frac{x}{\sigma x})^2+(\frac{y}{\sigma y})^2]}$$

Our stimulus, which is the observed star field is given by:

$$S = \sum_{i=1}^{N} A_i \delta(x - x_i)\delta(y - y_i)$$

where A_i denotes how bright each star is, and x_i, y_i denotes the position of the ith star. The flux from each star is then given by:

$$F = S * \phi$$

[3]For a color image see www.ugastro.berkeley.edu/kirsten

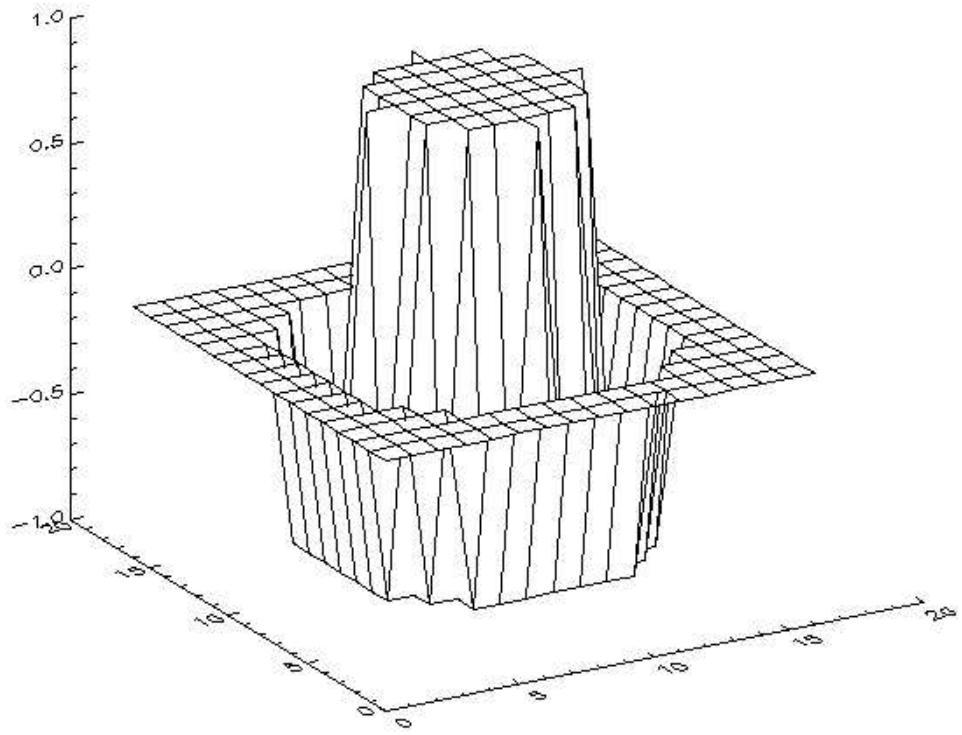

Fig. 2.— Aperture used to extract signal from mosaic. The two dimensional image is displayed in three dimensions, with the third corresponding to the value of the pixel. Note that the area of the adjacent moat is equal to the area of the raised, circular surface.

or,

$$F(x,y) = \int_{x_1}\int_{y_1} dx_1\, dy_1 \sum A_i \delta(x_1 - x_i)\delta(y_1 - y_i)\phi(x - x_i, y - y_i)$$

Mosaics were made of the cluster, standard stars and control field. Each image was convolved and the number of counts for each star extracted. Counts were converted into photoelectron counts using a gain factor[4] of $\frac{1}{20}$. Since the apparent magnitude of the standard stars was known, it was possible to compute the offset in each band. From Lab 3:

$$m^* = m_{*known} + 2.5\log_{10}\left(\frac{N_{*known}}{t_{*known}}\right) - 2.5\log_{10}\left(\frac{N^*}{t^*}\right)$$

[4]Computed in Lab 3.

Using a star of 0 magnitude as our known star, the offset was computed from:

$$m^* = -2.5 \log_{10}\left(\frac{N^*}{t^*}\right) + 2.5 \log_{10}\left(\frac{N_{*known}}{t_{*known}}\right)$$

$$m^* = -2.5 \log_{10}\left(\frac{N^*}{t^*}\right) + offset$$

Since we would expect that a count of 1 photoelectron for a 1 second exposure (the effective exposure time of our mosaic) could be attributed to Poisson noise, we can set a lower limit for the minimum observable magnitude equal to the offset. That is when $N^* = 1$:

$$m^* = offset$$

The flux was computed for each star in janskys using the values values for Vega (a zero apparent magnitude star) of $F_J = 1570$ Jy, $F_H = 1020$ Jy, and $F_K = 636$ Jy, and by using the equation for flux:

$$F_\nu^* = F_{\nu,Vega} + 2.5 \log_{10}(N^*)$$

The flux versus photoelectrons were plotted and a Least Squares Fitting was done. Observation of these plots indicated a potential discrepancy in the J band data, which failed to produce a flux of zero at zero photoelectron counts. Initially, the problem existed for both the H and J bands, but after reobserving the cluster and standards stars, errors in the initial data acquisition were corrected for the H band. Unfortunately, the J band still exhibited the same flaws. As a second check, our offset was compared to the results of Lada *et al.* Lada *et al* reported their detection limits (5σ) to be 16.5 magnitudes in the J band, 15.5 magnitudes in the H band, and 14.5 magnitudes in the K band. These offsets were used to make a prediction of where our magnitudes versus photoelectrons points might fall. The match was almost perfect in the H band, differing by .1 magnitudes (yielding 1.1 times larger number of photoelectron counts); fairly close in the K band, differing by .3 magnitudes (yielding 1.3 times larger number of photelectron counts); and significantly higher in the J band, differing by 1.4 magnitudes (yielding 3.63 times larger number of photoelectron counts). Both flux vs. phototelectron counts and magnitude vs. photoelectron counts are plotted in Figure 3 for all bands.

Using the calculated offsets, the magnitudes for 50 stars in each cluster were calculated. The values for the J band are listed in Table 1, the values for the H band are listed in Table 2, and the values for the K band are listed in Table 3. Any computed magnitudes dimmer than the offset cannot be considered valid stellar sources, since we should not be able to detect a star with a magnitude fainter than our offset. This means that in Table 1, stars 28-50 are not valid stellar sources, according to our original offset calculation. In fact, since the registered counts suggest an average detection of less than one photoelectron per second, it is possible that the signal register was due to Poisson noise. The only way to be certain if a signal had been detected would be to compute the signal to noise ratio for that particular point on the mosaic and compare, a very

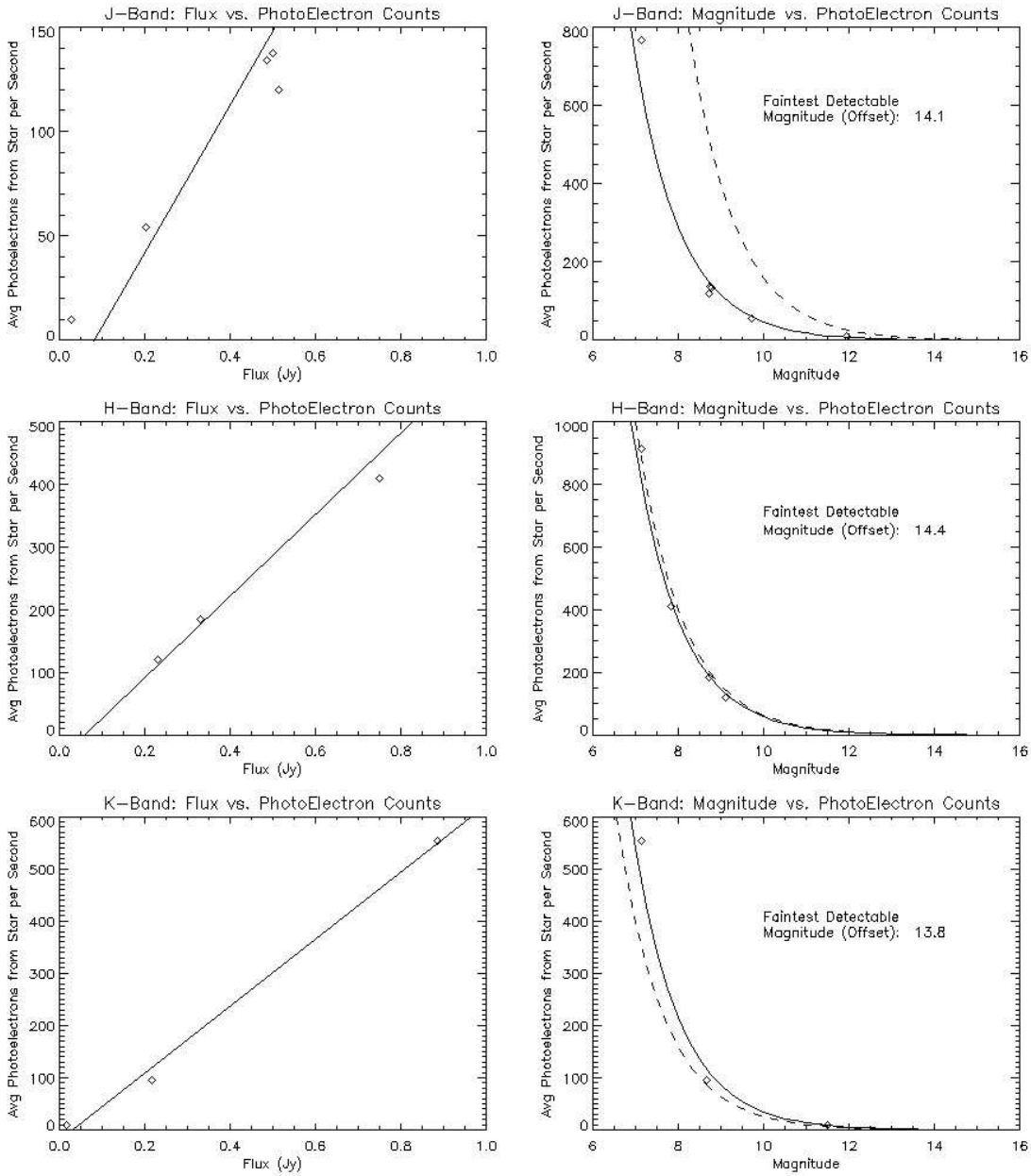

Fig. 3.— Flux vs. Photoelectron Counts and Magnitude vs. Photoelectron Counts in J, H, and K bands for standard stars. Flux is the computed from the number of photoelectrons received. Magnitudes are the known apparent magnitudes of the stars. Dashed line is a prediction based on faintest observable magnitudes of: m_J=15.5, m_H=14.5, m_K=13.5 (Lada *et al*). Note that J band deviates significantly from zero flux at zero photoelectron counts, and recorded number of photoelectrons differ significantly from predicted value values for corresponding magnitudes.

difficult task indeed! We can, however, observe that the location of faint signals in the J band reside at locations in the K and H bands where there was a strong signal, suggesting that we did indeed detect photons from a stellar source.

To demonstrate that we did indeed find a cluster, we needed to show that there was a statistically significant number of stars in the region. We used the control field as representation of the average surface density of stars for the Milky Way cluster. The control field was observed in the K band for the same amount of time as the cluster in the K band. Figure 4 plots a histogram of the magnitudes of the observed stars for both the cluster region and the control field. Our cluster field had 70% more stars than our control field, a significant amount more!

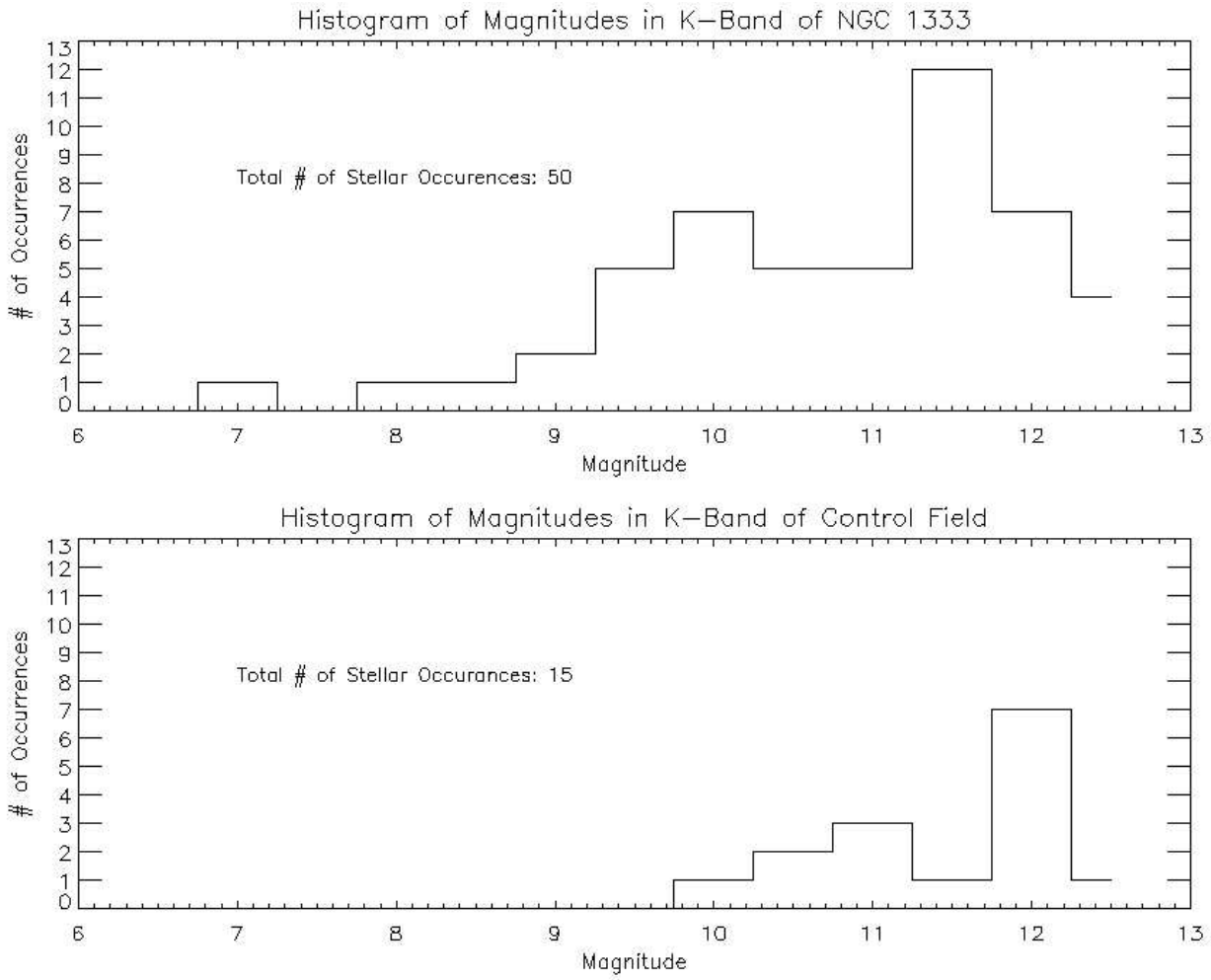

Fig. 4.— Histogram of Stellar Magnitudes in K Band for both cluster region and control field; 70% more stars were found in the cluster region.

Table 1: J Band Apparent Magnitudes

Star No.	Counts (secs)	m_J (uncorrected)	Star No.	Counts (secs)	m_J (uncorrected)	Star No.	Counts (secs)	m_J (uncorrected)
1	2444	8.92	18	53	13.07	35	15	14.43
2	1419	9.52	19	53	13.07	36	14	14.49
3	476	10.70	20	50	13.13	37	14	14.50
4	460	10.74	21	48	13.17	38	14	14.53
5	400	10.89	22	47	13.21	39	12	14.64
6	301	11.20	23	30	13.69	40	12	14.69
7	235	11.46	24	27	13.80	41	11	14.71
8	229	11.49	25	26	13.83	42	11	14.73
9	213	11.57	26	21	14.08	43	11	14.76
10	202	11.63	27	20	14.09	44	10	14.82
11	128	12.12	28	19	14.20	45	10	14.84
12	96	12.43	29	18	14.21	46	9	14.93
13	89	12.51	30	18	14.21	47	9	15.01
14	86	12.56	31	18	14.24	48	8	15.02
15	83	12.59	32	18	14.25	49	8	15.05
16	70	12.77	33	17	14.31	50	8	15.05
17	67	12.82	34	15	14.40			

Table 2: H band

Star No.	Counts (secs)	m_H (uncorrected)	Star No.	Counts (secs)	m_H (uncorrected)	Star No.	Counts (secs)	m_H (uncorrected)
1	8003	7.89	18	146	12.24	35	54	13.32
2	3053	8.94	19	145	12.25	36	53	13.33
3	1423	9.77	20	145	12.25	37	49	13.42
4	986	10.17	21	136	12.32	38	42	13.58
5	938	10.22	22	112	12.52	39	42	13.59
6	730	10.49	23	108	12.56	40	41	13.62
7	703	10.53	24	103	12.62	41	40	13.63
8	567	10.77	25	98	12.68	42	39	13.67
9	551	10.80	26	96	12.70	43	35	13.79
10	472	10.97	27	73	12.99	44	33	13.86
11	393	11.17	28	69	13.05	45	32	13.90
12	332	11.35	29	68	13.06	46	31	13.93
13	332	11.35	30	64	13.13	47	29	13.98
14	309	11.43	31	62	13.17	48	27	14.05
15	232	11.75	32	62	13.18	49	26	14.12
16	217	11.81	33	58	13.24	50	26	14.12
17	173	12.06	34	55	13.30			

Table 3: K band

Star No.	Counts (secs)	m_K (uncorrected)	Star No.	Counts (secs)	m_K (uncorrected)	Star No.	Counts (secs)	m_K (uncorrected)
1	10335	7.05	18	425	10.51	35	120	11.88
2	3844	8.12	19	372	10.65	36	115	11.95
3	1935	8.86	20	357	10.69	37	113	11.95
4	1178	9.40	21	344	10.74	38	110	11.97
5	1129	9.45	22	271	10.99	39	108	11.99
6	1037	9.54	23	259	11.04	40	94	12.14
7	863	9.74	24	257	11.05	41	91	12.18
8	845	9.76	25	224	11.20	42	90	12.19
9	747	9.89	26	196	11.35	43	90	12.19
10	736	9.91	27	185	11.41	44	87	12.23
11	628	10.08	28	160	11.57	45	71	12.46
12	596	10.14	29	153	11.62	46	70	12.46
13	590	10.15	30	146	11.67	47	68	12.50
14	567	10.19	31	142	11.69	48	67	12.52
15	534	10.26	32	132	11.77	49	65	12.54
16	495	10.34	33	128	11.80	50	61	12.61
17	450	10.44	34	122	11.85			

A color-color diagram was constructed using the calculated apparent magnitudes in the J, H and K bands for each star. The H-K Magnitudes were plotted versus the J-H Magnitudes. A program was constructed which correlated the locations of the stars in all three bands. Since some stars were to faint to register in all three bands, the program prompted the user to verify if a star in two different images was indeed the same star. Then, based on these locations, the values were subtracted, and the location noted to assure that the same H-K value and J-H value was plotted for its corresponding star.[5] The end result was a total of 33 stars extracted in the J, H and K bands out of the original 50. Even though, initially, some of the detected stars in the J band were questionable, the fact that the signals were separately extracted and still lied at exactly the same location in all three bands gave confidence to the assumption that a star had indeed been detected (in addition to the high signal to noise ratio). The H-K vs J-H values for main sequence stars[6], and the reddening bands[7] were also plotted, using the differences in the ratio of extinctions as the rise and run values for the slope. Figure 5 demonstrates these results.

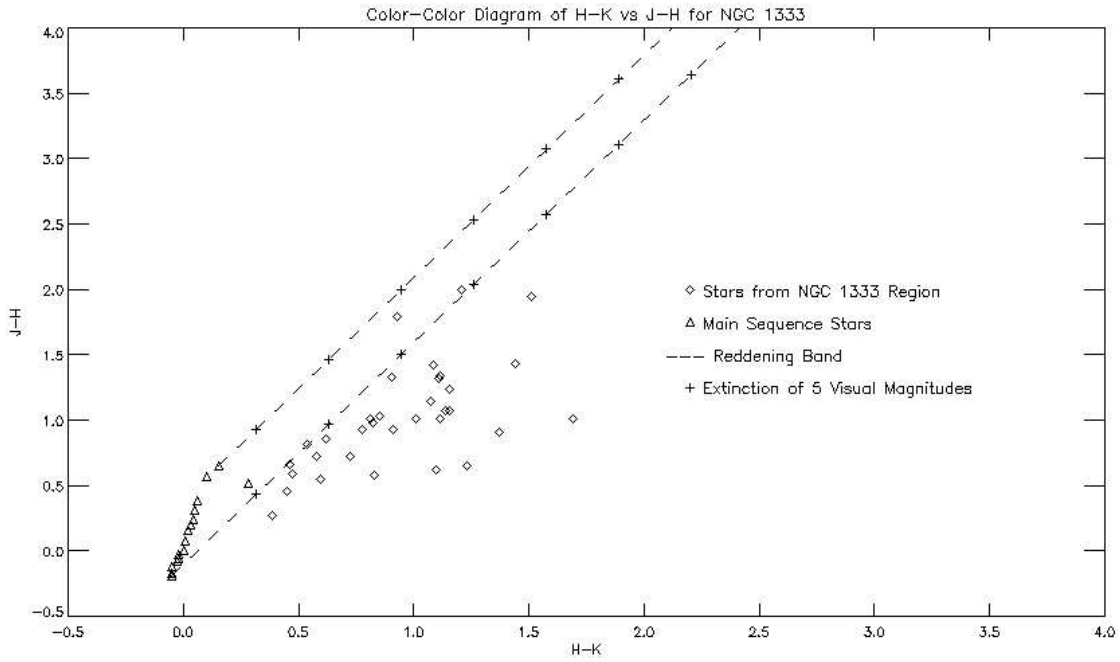

Fig. 5.— Color-Color Diagram of H-K vs. J-H for NGC 1333. Plotted stars from NGC 1333 Region were regressed down to the main sequence to determine the average amount of reddening of the cluster in the visual band.

[5]Only mosaics were shared by group. Since individual programs were written, and more than one set of data used, results of group may vary.

[6]Values obtained from Table 4, Lab 4 Handout.

[7]Values obtained from Table 3, Lab 4 Handout.

In order to determine the ratio of average amount of reddening of the cluster in each band to the visual band, each star from the cluster was regressed back down to the main sequence along a line parallel to the reddening band. This distance was then divided by the distance corresponding to one magnitude of of extinction to determine the average number of magnitudes extincted in the visual band; A_V was found to be 18.25 magnitudes[8]. The average value of A_V was used, as opposed to the individual values for each star, because of the wide scatter of points over 15 magnitudes of extinction. However, if our J band magnitudes are indeed dimmer, as suspected, we would expect to calculate a higher J-H value for each star, which would correlate to a lower number of extincted visual magnitudes. Using the given values for A/A_V, the number of extincted magnitudes in the J, H, and K bands were computed; these values were found to be 5.14, 3.19 and 2.04 magnitudes, respectively. Table 4 lists these corrected magnitudes along with the uncorrected magnitudes for the labeled stars in Figure 6 in the J, H, and K bands.

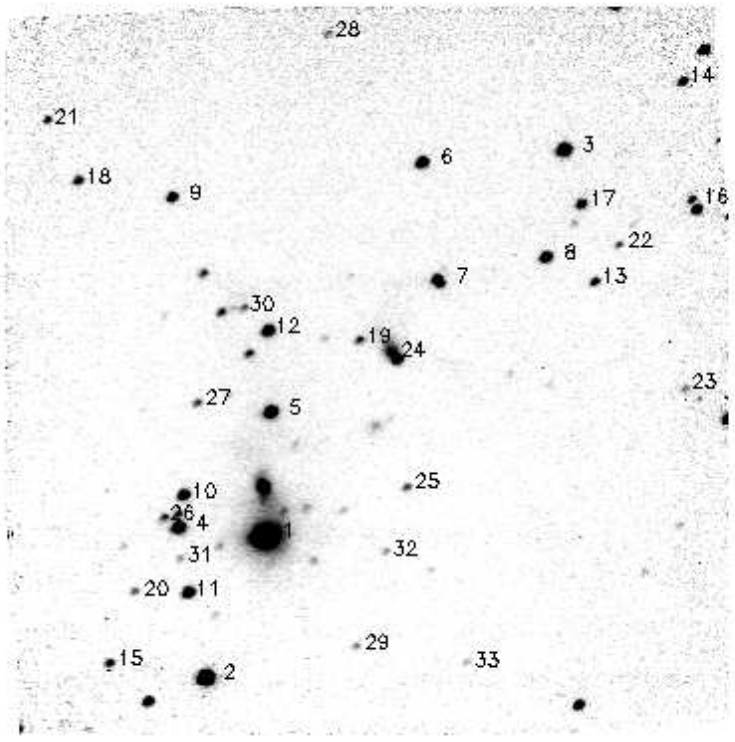

Fig. 6.— Stars in NGC 1333 cluster. Extinction corrected and uncorrected magnitudes are listed in Table 3 for J, H, and K bands. Displayed image is in the K band.

[8]This value is much larger than the average value of 6.2 ± 3.9 visual magnitudes of extinction for the cluster reported by Lade *et al.*

Table 4: Means and Standard Deviations: tabulated results of first data collection

Star No.	m_J	m_J corrected	m_H	m_H corrected	m_K	m_K corrected
1	8.92	3.66	7.89	4.63	7.04	4.95
2	9.52	4.25	8.94	5.68	8.11	6.03
3	10.70	5.44	9.77	6.50	8.86	6.77
4	10.89	5.63	10.17	6.90	9.45	7.36
5	11.20	5.94	10.22	6.96	9.40	7.31
6	11.46	6.20	10.53	7.27	9.76	7.67
7	11.49	6.23	10.77	7.50	10.19	8.10
8	12.12	6.86	10.80	7.53	9.89	7.80
9	11.63	6.37	10.97	7.70	10.51	8.42
10	12.59	7.33	11.17	7.90	10.08	7.99
11	12.77	7.51	11.35	8.08	9.91	7.82
12	12.43	7.17	11.43	8.16	9.74	7.65
13	12.56	7.30	11.74	8.47	11.20	9.11
14	12.82	7.56	11.81	8.55	10.69	8.60
15	13.07	7.81	12.06	8.79	11.05	8.96
16	12.51	7.25	12.24	8.97	11.85	9.76
17	14.20	8.94	12.25	8.98	10.74	8.65
18	14.24	8.98	12.25	8.99	11.04	8.95
19	13.17	7.91	12.32	9.05	11.69	9.61
20	13.07	7.81	12.52	9.26	11.92	9.83
21	13.80	8.54	12.56	9.30	11.41	9.32
22	13.21	7.95	12.62	9.35	12.14	10.05
23	13.13	7.87	12.68	9.41	12.23	10.14
24	14.49	9.23	12.70	9.43	11.77	9.68
25	14.31	9.05	12.99	9.73	11.88	9.79
26	14.21	8.95	13.06	9.80	11.99	9.90
27	14.08	8.82	13.17	9.91	11.80	9.71
28	13.83	8.57	13.18	9.91	11.95	9.86
29	13.83	9.38	13.30	10.03	12.19	10.10
30	14.64	9.14	13.33	10.07	12.19	10.10
31	14.40	9.17	13.42	10.15	12.61	10.52
32	14.43	9.43	13.62	10.35	12.46	10.37
33	14.69	8.99	13.63	10.37	12.54	10.45

Since the distance to the cluster was known, 320 pc, the absolute magnitude of the stars was computed in the K band using the relation:

$$M_K = m_{K,corrected} - 5\log_{10}(d) + 5$$

The J-K values were also corrected and plotted on a color-magnitude diagram (Figure 7). It is clear that the de-reddening caused a significant shift in the absolute magnitudes of our K band stars. It is, however, unexpected that this correction would cause such a significant shift in the J-K apparent magnitudes (although we would expect some shift). Again, this result is likely due to the initial errors in the J band offset calculation. Since our initial m_J was brighter than expected, our plotted J-K would result in lower values than expected.

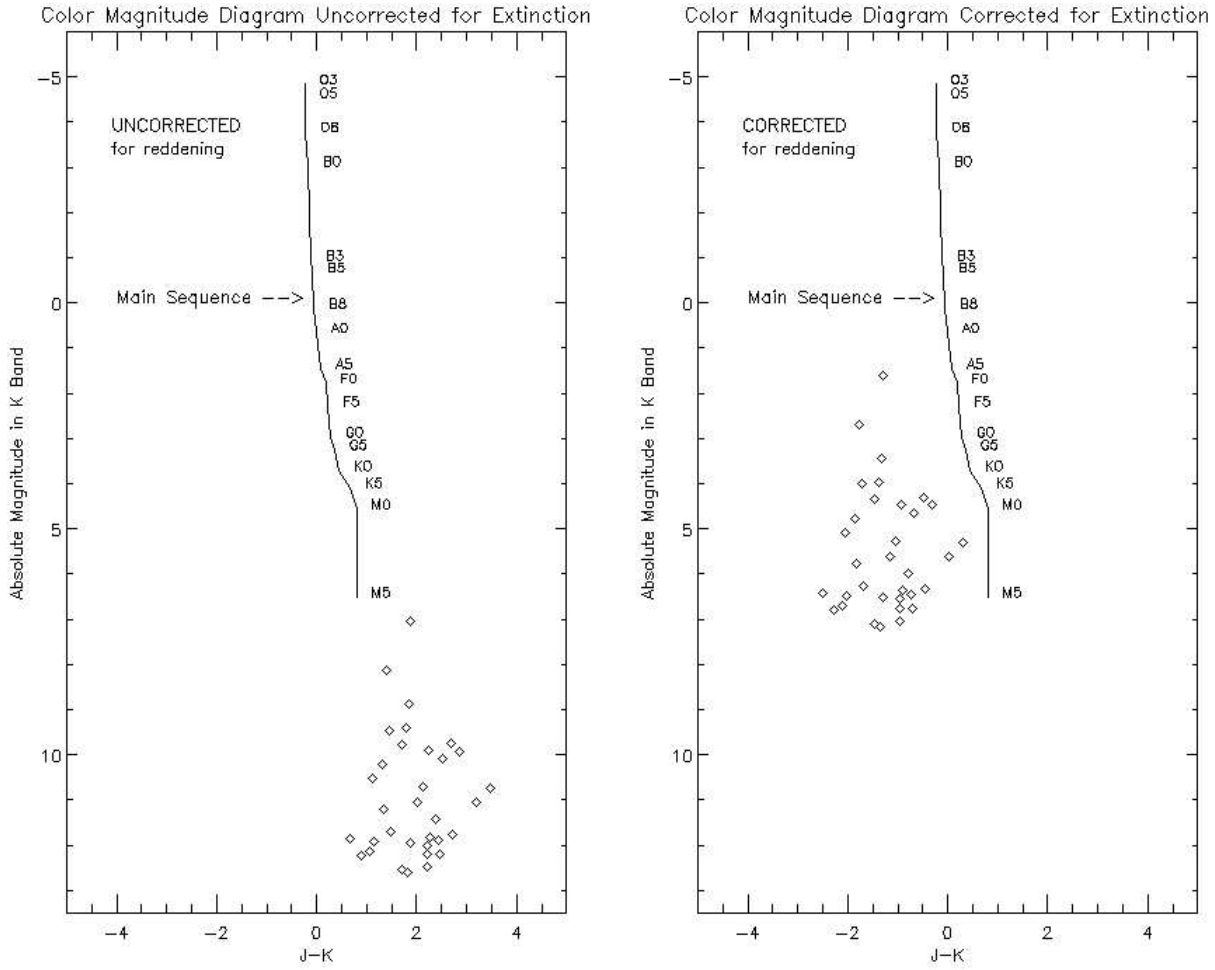

Fig. 7.— Color-Magnitude diagrams for NGC 1333, uncorrected for extinction and corrected for extinction. Main sequence stars were plotted in order to determine the types of stars in the cluster.

The corrected color-magnitude diagram provides interesting information when the locations of main sequence stars[9] are plotted. The stars which reside south of the main sequence line have either not yet finished forming and begun their ascent up the main sequence or are brown dwarfs. By observing where the brightest star in our star forming region lies, we can determine the spectral type of that star. The spectral type of our brightest star provides direct information about its mass, and thus allows us to determine its age. Since a larger, brighter star ascends the main sequence more rapidly than a lower mass star, we can use the age of the star as an estimate of the age of the cluster.

The brightest star in NGC cluster was determined to be a A5 type star, which has a mass of 2.0 solar masses. The mass-luminosity relationship[10]:

$$t = t_{*known} \left(\frac{M}{M_{*known}} \right)^{1-\alpha}$$

Using the sun as or t_{*known} (4.52 x 10^9 yr) and M_{*known}, and the value of 3.5 for α, the age of our star was determined be 8 x 10^8yr. This value is quite large compared to the age of 1-2 x 10^6 yr Lada *et al* calculated.

4. CONCLUSIONS

Although the result for the age of NGC 1333 was disappointingly high, it is clear how photons provide insight into the many mysteries of our galaxy and stellar formation. However, it is apparent that a significant error plagued the results of my observations. It would have been beneficial to take multiple sets of data in the different bands to determine the true offset of the J band (and verify those in the H and K bands), and also to check for any possible human errors in logging information, creating mosaics, etc. I think this experiment demonstrates the importance of the repeatability of of one's conclusions. It is unlikely that if I performed the same experiment 10 more times that I would come up with these same results each time. Chances are that I would come closer to the actually age of the cluster, within some error range. However, I highly doubt that the errors in this experiment are due to Poisson noise, thermal fluctuations, etc. Chances are that some human error took place, which further experiments might reduce or eliminate.

---

[9]Using Table 4 from Lab 4 for the J-K and M_K values. $M_K = M_V - (V - K)$

[10]Carroll, Bradley & Ostlie, Dale

5. REFERENCES

Carroll, Bradley W., Dale Ostlie, A. *An Introduction to Modern Astrophysics.* Addison-Wesley Publishing Co., 1996.

Lada, Charles J., Alves, Joao, and Lada, Elizabeth A. 1996, ApJ, 111.

Taylor, John R. *An Introduction to Error Analysis.* Sausalito: University Science Books, 1997.